Polymer Chemistry

ROYAL SOCIETY OF CHEMISTRY

PAPER

View Article Online
View Journal | View Issue

Cite this: *Polym. Chem.*, 2025, **16**, 1248

Synthesis of novel D–π–A-based photosensitive alkoxyamine: application of two-photon polymerization *via* nitroxide-mediated photopolymerization†

Nam Hoai Nguyen,‡[a] Xingyu Wu,‡[b] Yohann Guillaneuf,[a] Arnaud Spangenberg,[b] Didier Gigmes *[a] and Jean-Louis Clément *[a]

Received 2nd December 2024,
Accepted 29th January 2025

DOI: 10.1039/d4py01377h

rsc.li/polymers

We present an efficient method for surface customization using a novel D–π–A-based photosensitive alkoxyamine. The D–π–A-based chromophore group exhibits remarkable efficiency in the homolytic cleavage of the >NO–C bond enabling the production of well-defined structures through two-photon stereolithography (TPS). Furthermore, we show that surface customization can be achieved in a second step, owing to the "living" character originating from the alkoxyamine and *via* a Nitroxide Mediated PhotoPolymerization (NMP2) process. Additionally, we investigated how TPS-related parameters such as wavelengths and laser power influence the re-polymerization step.

1. Introduction

Two-photon stereolithography (TPS) is an advanced 3D printing method that relies on the non-linear absorption of light to create complex and three-dimensional microstructures.[1–3] This technique enables the fabrication of 2D/3D microstructures with feature sizes reaching sub-100 nm scales, opening up numerous promising applications such as high-density 3D optical data storage,[4,5] biomaterials,[6] and 3D sensors.[7,8] Typically, polymer materials used in TPS-produced microstructures undergo conventional radical photopolymerization,[9] leading to polymer networks with "dead" chains that are challenging to reactivate in a straightforward manner, thus limiting the ability to adjust polymer properties through post-modification processes.[1]

To enhance the diverse chemical functionalities of TPS-printed microstructures, it is imperative to propose new strategies aimed at tuning surface properties such as adhesion, wetting characteristics, permeability to gases or liquids, and biocompatibility. Surface functionalization of printed microstructures can be achieved using polymer chains terminated with unreacted vinyl bonds, functional groups, or residual photoinitiators.[10,11] However, the limited concentration of unreacted moieties or the sparse density of residual functional groups may restrict reactivity with other monomers and spatial resolution.[12,13]

Recently, the development of photo-reversible deactivation radical polymerization techniques like Atom Transfer Radical Polymerization (ATRP), Reversible Addition–Fragmentation chain-Transfer (RAFT) polymerization, and Nitroxide-mediated Polymerization (NMP) has provided advantages over conventional radical polymerization. These methods afford living, reactivable polymer chains with the added benefit of temporal-spatial control.[14] In this context, alkoxyamines gained increasing interest in photo-induced processes, particularly in Nitroxide-Mediated Photopolymerization (NMP2), owing to their use as both initiator and photo-controlling agent within a mono-component system. Unlike other methods such as ATRP or organometallic-mediated radical polymerization, NMP2 eliminates the need for metal complexes as catalysts,[15] and avoids the formation of undesirable colored thioester/thiocarbonate species characteristic of RAFT technique[16] where transparency is of crucial importance.

The success of the NMP2 process is essentially related to the physico-chemical behaviors under irradiation of both the photosensitive alkoxyamines and the parent nitroxide chemical structures. Many photosensitive alkoxyamines have been prepared by introducing the chromophore group to cyclic nitroxides such as 2,2,6,6-tetramethyl-1-piperidinyloxy (TEMPO),[17] or to linear nitroxides structures[18–20] including 2,2,5-trimethyl-4-phenyl-3-azahexane-3-nitroxide (TIPNO).[21,22]

Only a few photosensitive alkoxyamines, all related to TIPNO structure have been used in the surface functionali-

[a]*Aix Marseille Univ., CNRS, Institut de Chimie Radicalaire UMR 7273, Marseille, France. E-mail: didier.gigmes@univ-amu.fr, jean-louis.clement@univ-amu.fr*
[b]*Institut de Science des Matériaux de Mulhouse (IS2M), CNRS – UMR 7361, Université de Haute-Alsace, France Université de Strasbourg, 15 rue Jean Starcky, 68057 Mulhouse, France*

†Electronic supplementary information (ESI) available. See DOI: https://doi.org/10.1039/d4py01377h

‡These authors contributed equally.

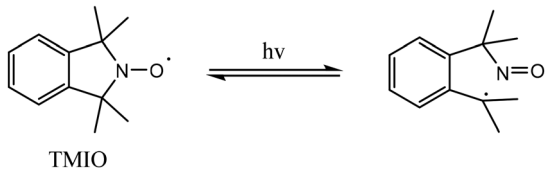

TMIO

Scheme 1 Photochemically induced α-cleavage of TMIO.

zation of 2.5D structures.[21,22] However, in some cases, acyclic structures may lead to competitive cleavages that affect the NMP2 process.[19] The selection of the persistent nitroxide is then crucial as it may profoundly impact the reactivity of the corresponding photosensitive alkoxyamines and the efficiency of the re-polymerization step. 1,1,3,3-Tetramethylisoindolin-2-yloxyl (TMIO) has been identified as a promising candidate for the preparation of photosensitive alkoxyamines due to its reversible photochemically-induced α-cleavage of the nitroxide upon irradiation. Indeed, upon homolytic cleavage, the proximity between the resulting nitroso group and the carbon-centered radicals allows the regeneration of the initial nitroxide (Scheme 1).[23] However, the exploration of TMIO motif-based photosensitive alkoxyamines where the phenyl ring is embedded within the overall chromophore has been impeded by synthetic challenges in obtaining benzophenone, and xanthone TMIO-based photosensitive alkoxyamines.[24,25] In recent years, push–pull structures have emerged as efficient TPS initiators due to their exceptional photostability and high molar absorption coefficient for nonlinear phenomena.[26–28] Typically, these push–pull compounds are designed based on electron donors (D) and acceptors (A), arranged in symmetrical A–π–A, D–π–D, or asymmetrical A–π–D chromophores.[29–32] Particularly, the asymmetrical D–π–A configuration exhibits rigid planar structures[33] and strong π–π interactions, resulting in a significant enhancement of the dipole moment, in the intense absorption band (λ) and significant solvatochromism in the emission spectrum.

Therefore, in this work, we introduce a convenient four-step procedure for synthesizing a photosensitive alkoxyamine based on a cyclic nitroxide featuring a phenyl ring, namely tacrine-based photosensitive alkoxyamine bearing a D–π–A chromophore group, tailored for the TPS-NMP2 process. Additionally, we illustrate the presence of "living" chains within microstructures fabricated from a photocurable resin containing the D–π–A-based photosensitive alkoxyamine through a surface functionalization step. To gain insights into the behavior of the resulting macroalkoxyamines within the polymer matrix, we conduct thorough investigations by varying parameters such as two-photon wavelengths and laser power.

2. Experiments

2.1. Materials

All chemicals purchased from Sigma Aldrich, TCI, and Doug Discovery were used without further purification unless indicated otherwise. All reactions were monitored by thin-layer chromatography (Merck Silica Gel 60 F254) and visualized by UV light. Purification *via* column chromatography was performed using silica gel 60 Å (230–400 mesh) from Sigma Aldrich. The 2,2,5,5-tetramethylpyrrolidin-3-one (**1**) was synthesized according to the ref. 34 (see ESI†).

2.2. Characterization

2.2.1. Nuclear magnetic resonance. ^{1}H and ^{13}C NMR spectra were recorded on Bruker Avance III HD 400 spectrometer operating at 400 MHz and 100 MHz equipped with an Ultra-shield magnet and using deuterated chloroform ($CDCl_3$) + 0.03% trimethylsilane (TMS) as an internal reference. Chemical shifts (δ) are given in ppm for ^{1}H and ^{13}C NMR spectra. Multiplicity is indicated as follows: s (singlet); d (doublet); t (triplet); m (multiplet); dd (doublet of doublet). Coupling constants are reported in hertz (Hz).

2.2.2. High-resolution mass spectrometry (HRMS). The analyzes were carried out with a SYNAPT G2 HDMS mass spectrometer (waters) equipped with a pneumatically assisted atmospheric pressure (API) ionization source. The sample was ionized in positive electrospray mode under the following conditions: electrospray voltage: 2.8 kV; orifice voltage: 20 V; nebulization gas flow rate (nitrogen): 100 L h^{-1}. The high-resolution mass spectrum was obtained with a time-of-flight (TOF) analyzer. The exact mass measurement was performed in triplicate with external calibration. The sample is dissolved in 300 μL of dichloromethane and then diluted to $1/10^3$ in a methanol solution containing 3 mM of ammonium acetate. The extract solution is introduced into the infusion ionization source at a flow rate of 10 μL min^{-1}.

2.2.3. Fourier transformation infrared (FT-IR). FI-IR spectra were recorded using a PerkinElmer Spectrum Two FT-IR spectrometer with an ATR accessory.

2.2.4. UV-Visible spectroscopy. All UV-visible spectra were recorded using a single-beam Varian Cary 50 UV-visible spectrophotometer.

2.2.5. Electron paramagnetic resonance (EPR) spectroscopy. EPR analyses were conducted using a Bruker EMX EPR spectrometer. A 600 μl-solution of appropriate alkoxyamines in *tert*-butyl benzene with concentration at 10^{-4} M L^{-1} in an NMR standard tube was directly irradiated within the EPR cavity using the Hamamatsu LC8 UV lamp (ESI, Fig. S8†). O_2 was used as a radical scavenger. Spectra were recorded on Win EPR software. Photolysis yields are given as the percentage of nitroxide recovered (EPR signals intensities) relative to a concentration of 10^{-4} M.

2.2.6. Atomic force microscopy (AFM). AFM images were realized in tapping mode on a commercial Bruker Multimode AFM. High-quality etched silicon probes, RTESPA-300 presenting a nominal spring constant $k \sim 40$ N m^{-1}, were used to obtain images of surface topographies.

2.3. Photostructuration

The formulation of NMP2 resin for the fabrication of the lines and 2D microstructures (squares) as a bottom layer was simply

prepared by dissolving 2 wt% of the alkoxyamine **5** (see below) in pentaerythritol triacrylate (PETA), while the formulation for the surface modification was just trimethylolpropane triacrylate (TMPTA) alone. One drop of the formulation was deposited on a coverslip that was then transferred to a chamber holder for microfabrication. The coverslip was previously functionalized with 3-(triethoxysilyl) propyl methacrylate to enhance the adhesion of microstructures.

All microfabrication was carried out on a two-photon fabrication set-up. The set-up includes a Ti:Sapphire laser system (Coherent Chameleon Ultra II, pulse duration: 140 fs; repetition rate: 80 MHz), a microscope (Zeiss Observer D1), a piezo stage (PI Mars 300 μm^3) and dedicated software to optimize fabrication paths and control the fabrication (SimPoly). The objective (×40, NA: 0.65) and exposure time (10 ms per voxel) were used for the fabrication of microstructures. After laser exposure, the samples were developed with ethanol. The base squares were immersed in ethanol for one week to be ready for surface modification. The same setup as microfabrication was used for surface modification. After putting one drop of formulation onto microstructures, laser beam was focused on the surface of the square for modification under controlled atmosphere (N_2). The objective (×40, NA: 0.65) and exposure time (10 ms per voxel) were also used for the modification. After laser exposure, the samples were washed again with ethanol. The laser wavelengths and intensities for microstructures and their surface modification are specified in the manuscript.

3. Results and discussion

3.1. Synthesis of D–π–A-based photosensitive alkoxyamine

Tacrine nitroxide,[35] which is based on a TMIO-type nitroxide moiety, can be synthesized in three simple steps, facilitating the straightforward preparation of the corresponding photosensitive alkoxyamines. However, the UV profile of tacrine does not encompass wavelengths which are utilized in a TPS system. Therefore, a bromo-substituted derivative (**4**) has been first synthesized in a four-steps procedure (Scheme 2).

Table 1 Optimization of Friedlander reaction conditions for the synthesis of **2**

Entry	Solvent	Temperature (°C)	Time (hours)	Yield[a] (%)
1	1,2-Dichloroethane	80	3	30
2	1,2-Dichloroethane	80	18	30
3	Toluene	115	3	40
4	Toluene	115	18	60

[a] Isolated yield.

First, the Friedlander condensation between **1** and 2-amino-5-bromo benzonitrile in the presence of aluminum chloride as a Lewis acid gives **2**, according to an adaptation of the Kálai's method.[35] To optimize the reaction yield, various experimental conditions were investigated (Table 1). The best compromise was obtained for a prolonged refluxing time in toluene (entry 4, 18 hours and 60% yield).

Once nitroxide **3** was obtained by the oxidation of **2** using *m*-CPBA, the atom transfer radical addition (ATRA) was performed to generate the corresponding bromo alkoxyamine **4** with 60% yield. The ^1H and ^{13}C NMR and HR-MS spectra confirmed the formation of the bromo alkoxyamine **4** (ESI, Fig. S4†).

The extension of the π-structure was then obtained by coupling bromo alkoxyamine **4** and the phenyl acetylene compound *via* a Sonogashira reaction to afford the D–π–A-based photosensitive alkoxyamine **5**. Under deoxygenated conditions, phenylacetylene was reacted with bromo alkoxyamine **4** in presence of palladium complex and copper(I) bromide at 60 °C in triethyl amine to give photosensitive alkoxyamine **5** with 60% yield. The successful preparation of **5** was confirmed by the ^1H and ^{13}C NMR and HR-MS spectra (ESI, Fig. S5†). The new appearance of hydrogen atoms of the aromatic ring of the phenylethynyl group is shown at 7.48 ppm and 7.36–7.21 ppm corresponding to alkoxyamine **5**. Additionally, the characteristic signal of the –C≡C– bond was observed at 88.66 and 88.60 ppm on the ^{13}C NMR spectrum (see ESI Fig. S5†).

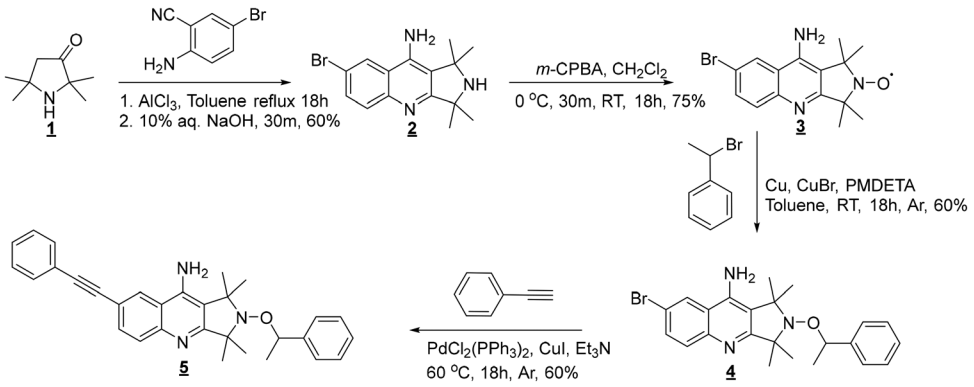

Scheme 2 Synthetic procedure of D–π–A-based photosensitive alkoxyamine **5**.

3.2. Photo-physical properties

As depicted in Fig. 1, compared to compound **4**, extending the chromophore group through the introduction of a phenyl group *via* an ethynylene (–CH≡CH–) linker to the alkoxyamine moiety induces a bathochromic effect on the absorption maximum for alkoxyamine **5**. Consequently, a red-shifted wavelength in λ_{max} was observed in the UV spectra of alkoxyamine **5** at 327 nm, compared to 308 nm for **4**. Moreover, the molar extinction coefficient at λ_{max} of **5** is more than double of that **4** (14 000 mol L^{-1} cm^{-1} and 6510 mol L^{-1} cm^{-1} for **5** and **4**, respectively, ESI Fig. S6 and S7†). UV spectra of alkoxyamine **5** exhibits two distinct bands: one below 309 nm corresponding to the π–π* transition and another between 300 and 370 nm assigned to the intramolecular charge transfer band. These UV-Visible absorbance properties suggest a potential application of photosensitive alkoxyamine **5** in two-photon lithography which was then investigated.

3.3. Photo-chemical properties

To determine whether the photodissociation process of a photosensitive alkoxyamine occurs through a selective >NO–C bond homolysis (Fig. 2A), we examined the behavior of alkoxyamines **4** and **5** by EPR under light irradiation. To avoid high-energy wavelengths that could induce destruction and potential side reactions of alkoxyamines in *tert*-butyl benzene solutions, only excitation wavelengths above 290 nm were used to investigate the photodissociation processes. Notably, EPR spectra revealed a clean homolytic cleavage of the >NO–C bond of **5** as no secondary radical species were detected (Fig. 2B) under continuous irradiation. Furthermore, a high recovery was observed for **5**, reaching a maximum of 72% after 2.5 hours (Fig. 2C). In addition, a significant increase in the nitroxide recovery is observable in comparison between **5** and **4** which reached only 35% after 4 hours under irradiation (Fig. 2C). This demonstrates the significant role played by the D–π–A chromophore group that facilitates the homolytic cleavage of the >NO–C bond within the alkoxyamine moiety. As expected for such a cyclic structure, the nitroxide exhibits an impressive stability even under long-term irradiation (7 hours). Hence, the UV absorbance properties and the photochemical properties show that the photosensitive alkoxyamine **5** may be a promising candidate for an NMP2 process conducted in a two-photon stereolithography system.

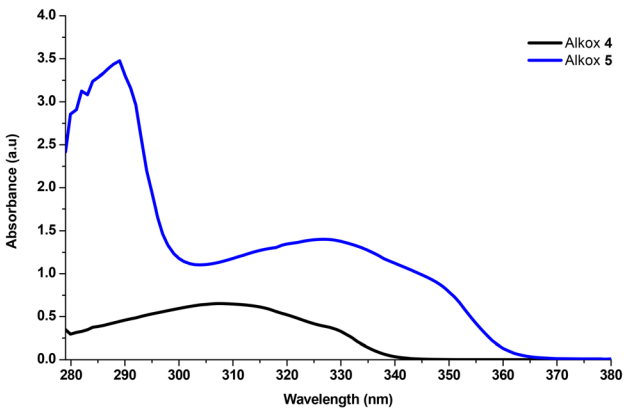

Fig. 1 UV – Visible spectra overlay of bromo tacrine-based alkoxyamine **4** and D–π–A tacrine TMIO-based alkoxyamines **5** in *tert*-butyl benzene with concentration = 1.0 × 10^{-4} M.

3.4. Two-photon polymerization properties

As outlined in the introduction, organic compounds based on the D–π–A architecture have gained significant attention concerning non-linear optical (NLO) phenomena particularly in two-photon polymerization. Inspired by its favorable photochemical properties, the D–π–A-based alkoxyamine **5** was employed in the frame of photo-reversible deactivation radical polymerization (photo-RDRP) for two-photon stereolithography. Unless otherwise stated, all fabrications and functionalizations were carried out with an exposure time of 10 ms per voxel, *i.e.* a writing speed of 14.3 μm s^{-1}.

3.4.1. Two-photon polymerization for the photosensitive alkoxyamine 5. The efficiency of a photoinitiator in two-photon stereolithography is often determined by measuring its two-photon absorption cross-section (σ) and the quantum yield of its reactive species (free radical, cation or anion) generation (Φ) in solution.[36] However, as explained by Baldacchini *et al.*,[37] this approach may not reflect the efficiency of the photoinitiator under experimental conditions in 3D fabrication. Another approach is based on determining the polymerization action spectrum by measuring the two-photon polymerization threshold power (P_{th}) as a function of excitation wavelength λ_{exc}. At a given wavelength,[37] P_{th} is defined as the minimum power required to initiate polymerization in TPS that withstands washing post-process. The plot $1/P_{th}^2$ against wavelength represents the two-photon polymerization action spectrum. The damage power P_{dam} corresponds to uncontrolled polymerization as evidenced by the observation of micro-explosions (Fig. S9†).

The two-photon initiating efficiency of **5** was thus first investigated by fabricating a series of lines on a glass support increasing laser power at a certain wavelength and using PETA as a multifunctional monomer, while keeping the other experimental conditions constant (writing speed, numerical aperture of the objective, *etc.*). As an example in Fig. S9,† the two-photon polymerization threshold power for 2 wt% of alkoxyamine **5** in PETA was estimated to be 14.5 mW at an excitation wavelength of 740 nm. This experiment was reproduced at different wavelenghts from 690 to 760 nm. Then, the threshold powers at each wavelength (from 690 to 760 nm) were plotted against wavelength to obtain the two-photon polymerization action spectrum (Fig. 3). The higher the value of $1/P_{th}^2$ is, the lower energy is required for two-photon polymerization, which reflects a better efficiency of a photoinitiator. Fig. 3 shows that two-photon polymerization occurs over a certain wavelength range from 690 nm to 760 nm for that specific photocurable resin (PETA + 2 wt% **5**) with the highest value of $1/P_{th}^2$ obtained at λ = 700 nm. The one photon UV-visible spectrum of **5** showed a higher absorbance at 345 nm than at 350 nm in

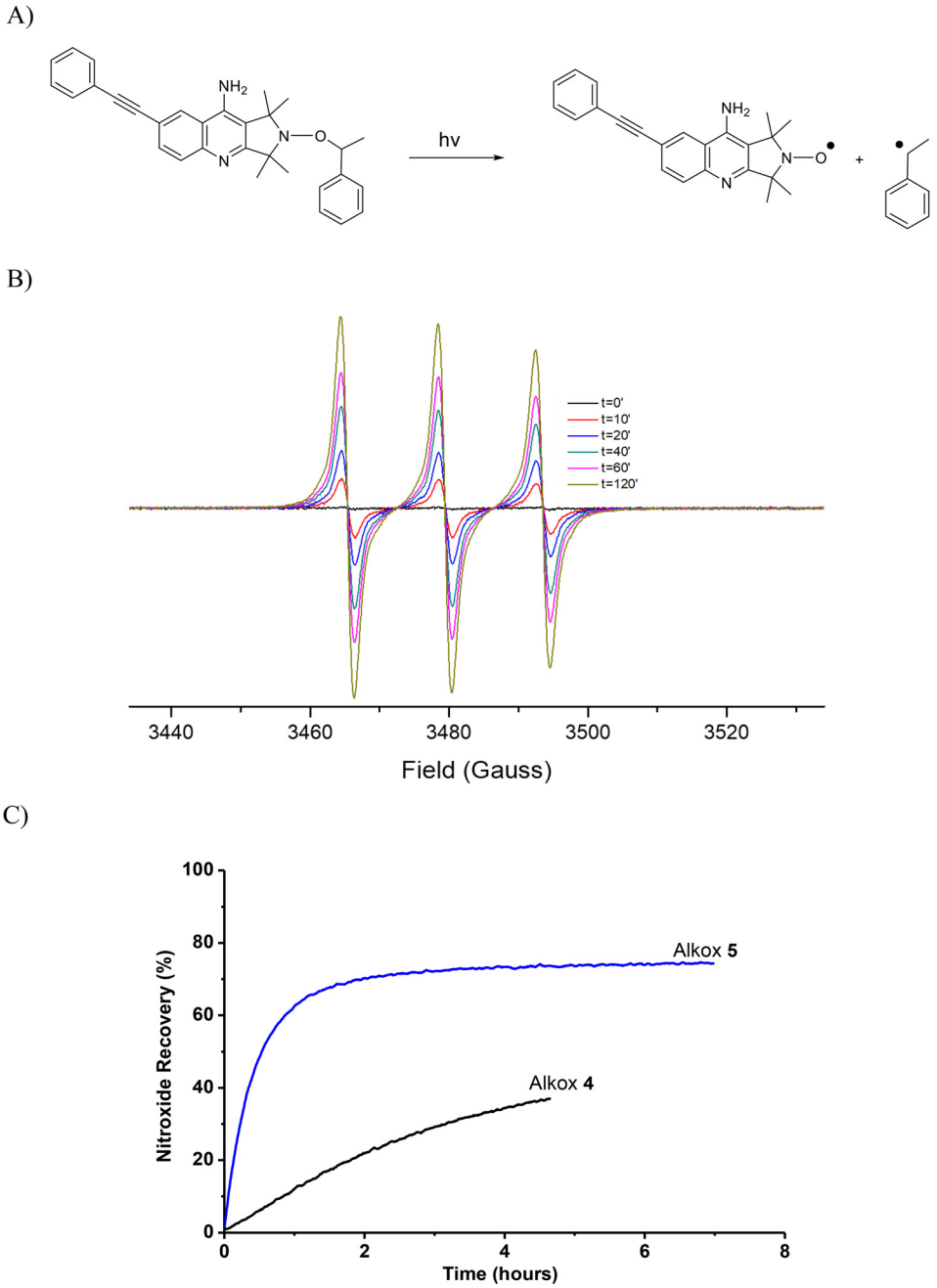

Fig. 2 (A) Schematic photodissociation reaction of photosensitive alkoxyamine **5**. (B) Evolution of the EPR spectrum of D–π–A-based alkoxyamines **5** during the first 140 minutes of irradiation (C) nitroxide recoveries obtained for bromo alkoxyamine **4** and D–π–A-based alkoxyamine **5** under UV irradiation using LC8 lamp at 10% of power (emission spectrum of this lamp in ESI, Fig. S8†).

tert-butyl benzene and in contrast a higher sensitivity of the system is situated at 700 nm for 2-photon polymerization action spectrum. Numerous factors can explained this slight discrepancy, the first being the fact that both experiments are conducted in a specific environment (solvent *vs.* monomers matrix). Besides, depending of the molecular structure of the photoinitiators, the electronic transitions can be one or two photon active.[38,39] Interestingly, while the radical quantum yield is generally believed to be independent of wavelength, recent studies conducted by Barner-Kowollik *et al.* have highlighting that the monomer to polymer conversion does not fully align with the absorption spectrum of the photoinitiator. The discrepancy between the absorption spectrum and the monomer conversion have been ascribed to an alternative photochemical path.[40] Very recently, similar observations have been also reported for controlled radical polymerization.[41]

3.4.2. 2D microfabrication and surface modification. To demonstrate the potential of alkoxyamine **5** for two-photon

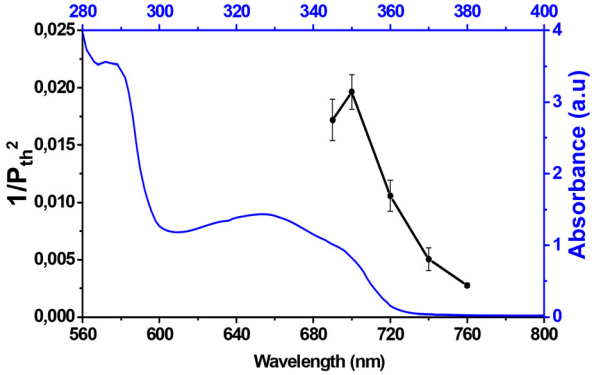

Fig. 3 UV-visible absorbance spectra of alkoxyamine **5** in *tert*-butyl benzene solution (1.0×10^{-4} M) (blue curve) and two-photon polymerization action spectra for PETA with 2 wt% alkoxyamine **5** (black line).

fabrication, a 2D microstructure (50×50 μm^2, Fig. S10†) was produced using a laser excitation power of 15.6 mW, close to the threshold power at 740 nm. These parameters though far from the range of highest initiating efficiency were used to avoid over production of initiating radicals and limit the degree of reticulation of the polymer network. Important reticulation may constrain the interpenetration between the first polymer network and thus with macro-alkoxyamine formed during the fabrication step and the new monomer added during the functionalization step.[22]

After immersing this microstructure in ethanol for one week to eliminate any unreacted monomer and photoinitiator, surface modification of this structure was conducted *via* two-photon irradiation owing to the formation of macro-alkoxyamine as depicted in Fig. 4. A drop of trimethylolpropane triacrylate (TMPTA) without any additional photoinitiators was applied onto this bottom square. Then, a series of lines were fabricated on its surface using wavelengths ranging from 690 nm to 760 nm under a nitrogen atmosphere (Fig. 4B). It should be noted that laser irradiation outside the top of the first manufactured layer does not induce polymerization (ESI Fig. S11†) showing that re-polymerization occurred from the living macro photosensitive alkoxyamines at the surface. The threshold powers at different wavelengths were determined and plotted against wavelength to generate the two-photon re-polymerization action spectrum for pure TMPTA (Fig. 4C). A good agreement between the two-photon polymerization (for the resin of PETA and **5**, Fig. 3) and two-photon re-polymerization (for pure TMPTA, Fig. 4) action spectra were observed, indicating comparable initiating behavior of alkoxyamine **5** and macro-alkoxyamine at different wavelengths. These results highlight the possibility of surface functionalization of microstructures *via* reactivable macro-alkoxyamines originated from the alkoxyamine-based photoresin (PETA + **5**).

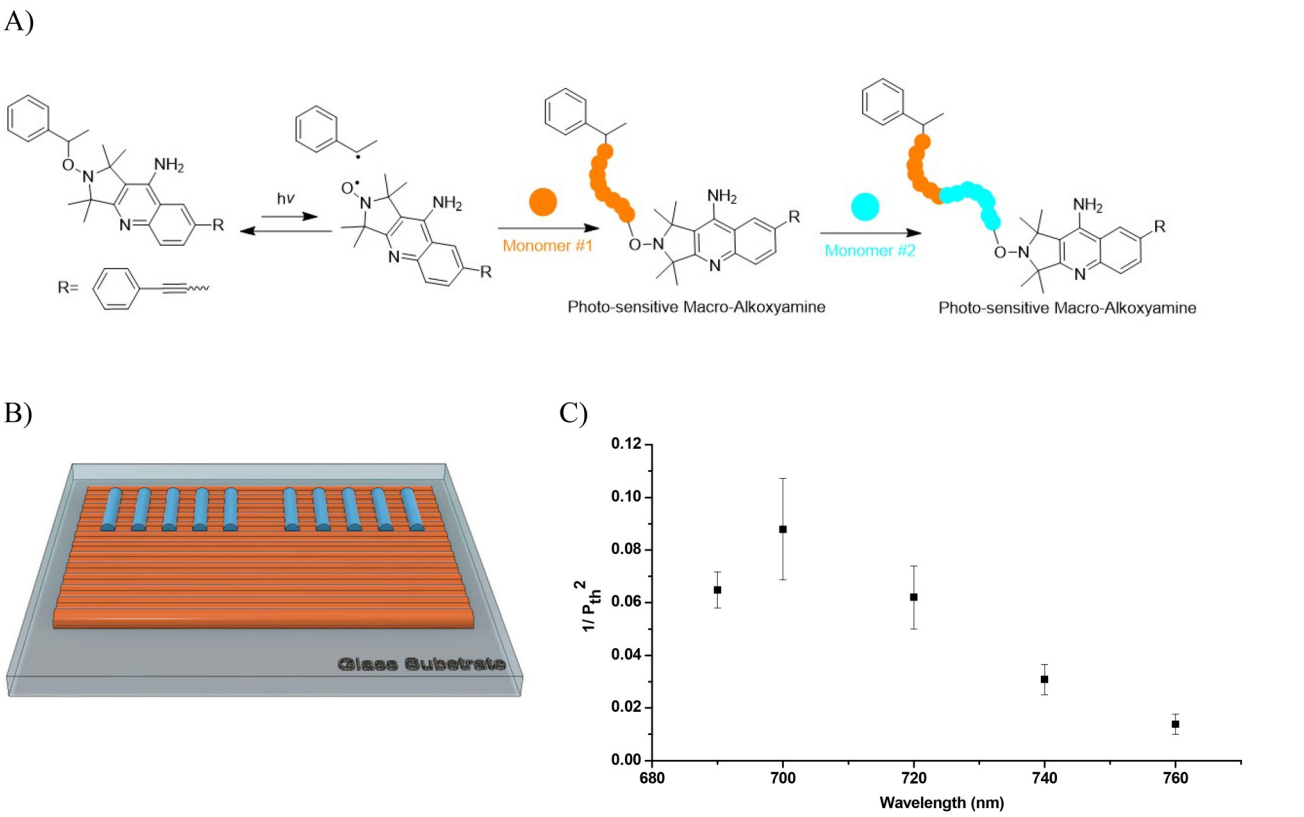

Fig. 4 (A) Schematic presentation of the NMP2 two-photon stereolithography fabrication and surface functionalization processes. (B) Schematic presentation of written lines on the first layer and (C) two-photon re-polymerization action spectrum for TMPTA without addition of external photoinitiator at a wavelength range from 690 to 760 nm, under N_2.

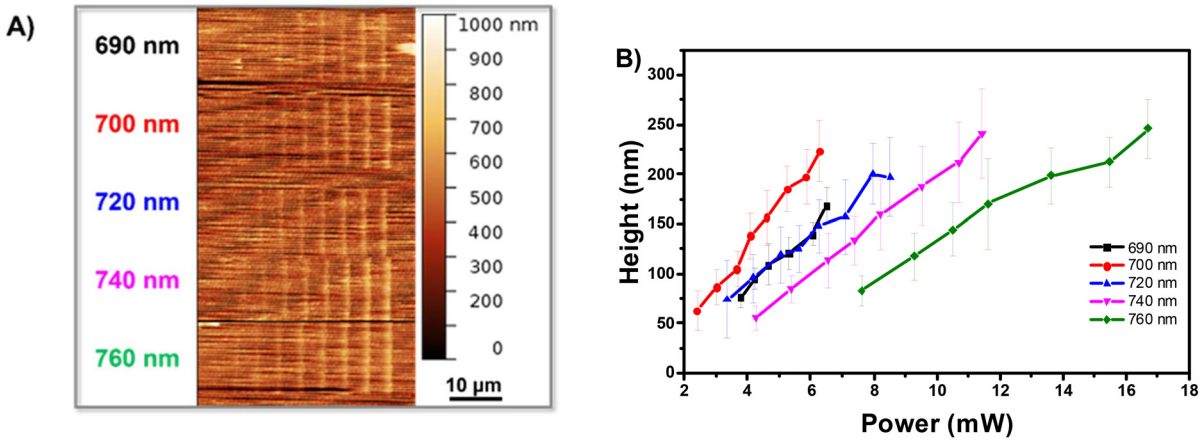

Fig. 5 (A) AFM image of the two-photon re-polymerization of a series of lines on the surface of a first square fabricated at 15.6 mW and 740 nm at: 690 nm, 700 nm, 720 nm, 740 nm, and 760 nm, exposure time = 10 ms with increasing the laser power (left to right) and (B) the evolution of the heights of written lines at different laser powers and wavelengths on the surface's bottom layer in the surface modification step.

3.4.3. Influence of writing parameters (power lasers and wavelengths) on surface modification. Above, we demonstrated that the bottom layer can be surface-modified using TPS in the presence of photosensitive macro-alkoxyamines. Two key parameters – laser powers and the excitation wavelength – directly influence the surface modification. Therefore, we examine here the effects of varying laser powers and two-photon excitation wavelengths on the height of the lines on the modified layer.

AFM images of written lines on the bottom square are illustrated in Fig. 5A clearly show that the heights of lines increase with an increasing laser intensity at each wavelength (Fig. 5B). For example, at λ = 700 nm, the heights increase from 63 (±3) nm to 224 (±8) nm when the laser intensities vary from 2.41 mW cm^{-2} to 6.28 mW cm^{-2}. Moreover, wavelengths have a strong influence on the heights of lines. One can notice that at the same intensity, the lines made at 700 nm are higher than those made at 690 nm and decrease at longer wavelengths, which can be explained by the plot of $1/P_{th}^2$ obtained for pure TMPA (Fig. 4C), *i.e.*, the initiating efficiency of macro-alkoxyamine in such conditions. Overall, the heights of lines can be adjusted between 60 and 230 nm, demonstrating the potential to realize surface functionalization at sub-micrometer feature sizes in a controlled manner by varying laser intensity or wavelength.

4. Conclusion

A novel D–π–A-based alkoxyamine **5** was conveniently synthesized using Sonogashira condition reaction from corresponding bromo precursor **4** in a single step. UV-Visible spectroscopy revealed red-shifted spectra bands and improved absorbance properties upon the introduction of the phenylethynyl group to the tacrine alkoxyamine moiety. The corresponding nitroxide formed upon irradiation exhibits significant stability even under prolonged irradiation (7 hours). The efficiency of photo-sensitive alkoxyamine **5** to initiate polymerization under a two-photon absorption process (from 690 to 760 nm) was demonstrated by fabricating 2D microstructures. Through an NMP2 process that led to reactive functionalities (*i.e.* photosensitive macro-alkoxyamines) at the surface, post-modification of the surface can be achieved with another monomer having different chemical features. The impact of the fabrication parameters (laser and wavelength) on these structures was investigated and showed a fine-tuning of the line height. It must be noted that the use of photosensitive alkoxyamine does not require the use of any other additive *via* a true mono-component system or the further addition of an initiator for the re-polymerization step. Therefore, the combination of NMP2 with two-photon stereolithography provides a powerful strategy to fabricate and reconfigure microstructures, but also to make multi-material by micro-printing.

Author contributions

The manuscript was written through contributions of all authors. All authors have given approval to the final version of the manuscript.

Data availability

Supplementary data for this article are present in the ESI.†

Conflicts of interest

There are no conflicts to declare.

Acknowledgements

The authors thank the Agence Nationale de la Recherche for financial supports (Project 3D CustomSurf ANR-19-CE06-0027;

project Mat-Light 4.0 ANR-21-EXES-0012, the latter being a French government grant managed by ANR under the France 2030 program). The authors thank Benjamin Leuschel for the helpful discussion regarding the AFM and SEM experiments.

References

1 C. Barner-Kowollik, M. Bastmeyer, E. Blasco, G. Delaittre, P. Müller, B. Richter and M. Wegener, *Angew. Chem.*, 2017, **129**, 16038–16056.
2 N. Hobeika, H. Chaumeil, R. Mhanna, M. Jin, X. Wu, A. Spangenberg, D. L. Versace, F. Morlet-Savary and J. P. Malval, *ChemPhysChem*, 2020, **21**, 2301–2310.
3 M. Hippler, E. Blasco, J. Qu, M. Tanaka, C. Barner-Kowollik, M. Wegener and M. Bastmeyer, *Nat. Commun.*, 2019, **10**, 232.
4 G. S. He, in *Progress in Optics*, ed. T. D. Visser, Elsevier, 2019, vol. 64, pp. 155–278.
5 S. Goswami, S. Cekli, E. Alarousu, R. W. Winkel, M. Younus, O. F. Mohammed and K. S. Schanze, *Macromolecules*, 2020, **53**, 6279–6287.
6 X. Wang, Z. Wei, C. Z. Baysah, M. Zheng and J. Xing, *RSC Adv.*, 2019, **9**, 34472–34480.
7 M. A. Abaddi, L. Sasso, M. Dimaki and W. E. Svendsen, *Microelectron. Eng.*, 2012, **98**, 378–381.
8 J. C. Williams, H. Chandrahalim, J. S. Suelzer and N. G. Usechak, *Adv. Photonics Res.*, 2022, **3**, 2100359.
9 Y. Yagci, S. Jockusch and N. J. Turro, *Macromolecules*, 2010, **43**, 6245–6260.
10 H. Ceylan, I. C. Yasa and M. Sitti, *Adv. Mater.*, 2017, **29**, 1605072.
11 A. S. Quick, A. de los Santos Pereira, M. Bruns, T. Bückmann, C. Rodriguez-Emmenegger, M. Wegener and C. Barner-Kowollik, *Adv. Funct. Mater.*, 2015, **25**, 3735–3744.
12 A. S. Quick, J. Fischer, B. Richter, T. Pauloehrl, V. Trouillet, M. Wegener and C. Barner-Kowollik, *Macromol. Rapid Commun.*, 2013, **34**, 335–340.
13 J. Zhang, H. Ding, X. Liu, H. Gu, M. Wei, X. Li, S. Liu, S. Li, X. Du and Z. Gu, *Small*, 2021, **17**, 2101048.
14 N. Corrigan and C. Boyer, *Trends Chem.*, 2020, **2**, 689–706.
15 S. Yamago and Y. Nakamura, *Polymer*, 2013, **54**, 981–994.
16 M. Hartlieb, *Macromol. Rapid Commun.*, 2022, **43**, 2100514.
17 S. Hu, J. H. Malpert, X. Yang and D. C. Neckers, *Polymer*, 2000, **41**, 445–452.
18 J. Morris, S. Telitel, K. E. Fairfull-Smith, S. E. Bottle, J. Lalevée, J. L. Clément, Y. Guillaneuf and D. Gigmes, *Polym. Chem.*, 2015, **6**, 754–763.
19 Y. Guillaneuf, D. Bertin, D. Gigmes, D. L. Versace, J. Lalevée and J. P. Fouassier, *Macromolecules*, 2010, **43**, 2204–2212.
20 Y. Guillaneuf, D.-L. Versace, D. Bertin, J. Lalevée, D. Gigmes and J.-P. Fouassier, *Macromol. Rapid Commun.*, 2010, **31**, 1909–1913.
21 S. Telitel, J. C. Morris, Y. Guillaneuf, J.-L. Clément, F. Morlet-Savary, A. Spangenberg, J.-P. Malval, J. Lalevée, D. Gigmes and O. Soppera, *ACS Appl. Mater. Interfaces*, 2020, **12**, 30779–30786.
22 M. Belqat, X. Wu, J. Morris, K. Mougin, T. Petithory, L. Pieuchot, Y. Guillaneuf, D. Gigmes, J.-L. Clément and A. Spangenberg, *Adv. Funct. Mater.*, 2023, **22**, 2211971.
23 S. E. Bottle, U. Chand and A. S. Micallef, *Chem. Lett.*, 1997, **26**, 857–858.
24 J. C. Morris, L. A. Walsh, B. A. Gomes, D. Gigmes, K. E. Fairfull-Smith, S. E. Bottle and J. P. Blinco, *RSC Adv.*, 2015, **5**, 95598–95603.
25 M. Herder and J. M. Lehn, *J. Am. Chem. Soc.*, 2018, **140**, 7647–7657.
26 Z. Faraji Rad, P. D. Prewett and G. J. Davies, *Microsyst. Nanoeng.*, 2021, **7**, 71.
27 M. Pawlicki, H. A. Collins, R. G. Denning and H. L. Anderson, *Angew. Chem., Int. Ed.*, 2009, **48**, 3244–3266.
28 V. Harinarayana and Y. C. Shin, *Opt. Laser Technol.*, 2021, **142**, 107180.
29 G. S. He, L.-S. Tan, Q. Zheng and P. N. Prasad, *Chem. Rev.*, 2008, **108**, 1245–1330.
30 M. Kivala and F. Diederich, *Acc. Chem. Res.*, 2009, **42**, 235–248.
31 A. S. Andersson, L. Kerndrup, A. Madsen, K. Kilså, M. B. Nielsen, P. R. La Porta and I. Biaggio, *J. Org. Chem.*, 2009, **74**, 375–382.
32 J. Kulhánek, F. Bureš, O. Pytela, T. Mikysek, J. Ludvík and A. Růžička, *Dyes Pigm.*, 2010, **85**, 57–65.
33 D. Zhang, J. Yang, C. Liu, S. Ye, Q. Zhang and R. Liu, *Int. J. Nanomed.*, 2021, **16**, 4901–4911.
34 D. M. Hodgson, C. D. Bray, N. D. Kindon, N. J. Reynolds, S. J. Coote, J. M. Um and K. N. Houk, *J. Org. Chem.*, 2009, **74**, 1019–1028.
35 T. Kálai, R. Altman, I. Maezawa, M. Balog, C. Morisseau, J. Petrlova, B. D. Hammock, L. W. Jin, J. R. Trudell, J. C. Voss and K. Hideg, *Eur. J. Med. Chem.*, 2014, **77**, 343–350.
36 P. J. Campagnola, D. M. Delguidice, G. A. Epling, K. D. Hoffacker, A. R. Howell, J. D. Pitts and S. L. Goodman, *Macromolecules*, 2000, **33**, 1511–1513.
37 T. Baldacchini, C. N. LaFratta, R. A. Farrer, M. C. Teich, B. E. A. Saleh, M. J. Naughton and J. T. Fourkas, *J. Appl. Phys.*, 2004, **95**, 6072–6076.
38 R. Zhou, J.-P. Malval, M. Jin, A. Spangenberg, H. Pan, D. Wan, F. Morlet-Savary and S. Knopf, *Chem. Commun.*, 2019, **55**, 6233–6236.
39 M. N. Nair, N. Hobeika, F. Calard, J.-P. Malval, S. Aloïse, A. Spangenberg, L. Simon, M. Cranney, F. Vonau, D. Aubel, F. Serein-Spirau, J.-P. Lère-Porte, M.-A. Lacourb and T. Jarrosson, *Phys. Chem. Chem. Phys.*, 2014, **16**, 12826–12837.
40 D. E. Fast, A. Lauer, J. P. Menzel, A.-M. Kelterer, G. Gescheidt and C. Barner-Kowollik, *Macromolecules*, 2017, **50**, 1815–1823.
41 M. Nardi, E. Blasco and C. Barner-Kowollik, *J. Am. Chem. Soc.*, 2022, **144**, 1094–1098.